19th Brazilian Congress of Thermal Sciences and Engineering
November 6th–10th, 2022, Bento Gonçalves - RS - Brazil

ENC-2022-0251
Estimation of Double Tsuji flames dimension based on experimental, analytical and numerical results

Jean A. Barbosa
Grupo de Mecânica de Fluidos Reativos, Instituto Nacional de Pesquisas Espaciais, Cachoeira Paulista - SP, Brazil
jean.barbosa@inpe.br
José C. de Andrade
Grupo de Mecânica de Fluidos Reativos, Instituto Nacional de Pesquisas Espaciais, Cachoeira Paulista - SP, Brazil
jose.andrade@inpe.br
Matheus P. Severino
Instituto de Ciências Matemáticas e de Computação, Universidade de São Paulo, São Carlos - SP, Brazil
matheus.severino@usp.br
Vinicius M. Sauer
Department of Mechanical Engineering, California State University , Northridge - CA, USA
vmsauer@csun.edu
Fernando F. Fachini
Grupo de Mecânica de Fluidos Reativos, Instituto Nacional de Pesquisas Espaciais, Cachoeira Paulista - SP, Brazil
fernando.fachini@inpe.br

Abstract. *This work goal is the estimation of Double Tsuji flame dimension using an experimental setup together with a 2D simulation through the commercial solver Fluent® and a scale model. This new configuration consists of a porous cylindrical burner, ejecting fuel radially and uniformly, in the middle of two impinging jets of oxidizer. It forms two counterflow regions, similar to the classical Tsuji burner, one upward and the other downward of the burner. The flame dimensions based on the scale model are related to a flame shape factor, the air-fuel stoichiometric relation and two Péclet numbers, one relative to the burner and the other to the impinging flow. In the numerical simulation, GRI3.0 was used as the kinetic mechanism and Fick's law for the species transport model. As this is a new burner configuration, besides the flame dimension estimation, it is important to confirm if Fluent® can be used to describe the physical aspects of the double Tsuji flame. Three fuel flow velocities and one oxidizer flow velocity are considered in the experimental tests. The experimental flame measurement was performed using a pixel-to-distance calibration on the flame photographic images. Due to the flame thickness, there is a region of increase in pixel value, so the flame is located between the two coordinates of the half maximum pixel value, named the lower and upper branches. The results show that the simplified scale model estimates well the location of the lower branch despite its simplicity. The highest deviation for the flame's length was 17.56 % and for the flame's height was 34.15 %, both for the biggest fuel flow velocity. The numerical simulation shows a better agreement with the experimental results than the scale model. In the counterflow region, the entire consumption of fuel and oxidizer is located between the two experimental branches. Moreover, the temperature peak is near the location of the maximum pixel value. However, the numerical simulation overestimated the flame length because it is not considered the oxidizer transportation in the z-axis, that will result in a more compact flame.*

Keywords: *double Tsuji burner, double Tsuji flame, laminar-diffusion flame*

1. INTRODUCTION

Counterflow flames have been extensively used to study the structure of diffusion flame. A classical type of burner that provides these flames is the Tsuji burner. It consists of a porous cylinder placed in an external stream of oxidizer. The region downward of the burner, where the oxidizer flow encounters the fuel flow, forms a counterflow flame (Tsuji and Yamaoka, 1967, 1969, 1971; Tsuji, 1982). The "backside" of the burner was not given special attention by Tsuji and his co-works. However, including the fuel ejection from the backside, the results showed a very elongated flame (Bianchin *et al.*, 2019). Far away from the burner, the fuel and oxidizer flows can be considered pararellel, resulting in only diffusion

of oxidizer to the flame. Changing the external oxidizer stream (forced convection) to a buoyancy-induced flow (natural convection), a more compact flame is formed (Donini *et al.*, 2020). The natural convection creates a perpendicular convection component to the flame, which brings more oxidizer to the flame. In short, the oxidizer transportation to the flame is lower in the forced convection case than in the natural convection case.

Based on these results, a new configuration that enhances the oxidizer transportation to the flame was proposed (Severino *et al.*, 2021). It was introduced another oxidizer flow in the opposed direction to that one present in the classical Tsuji configuration, i.e., a cylindrical burner in a counterflow. The two external flows create an impinging flow field that has the porous burner placed in the middle of the oxidizer flow. It forms two counterflow regions, one upward and the other downward the burner. Thus, the proposed configuration was named as the double Tsuji burner, and the flame established in it, as the double Tsuji flame. This novel configuration expands the study on entrainment, because the entrainment is directly controlled (externally controlled) by the system boundary conditions, specifically by the velocity of the oxidant jets. It was also observed that the oxidizer is transported by convection in the first 3/5 of flame length and, in the rest of it (the last 2/5), the fuel is transported by convection to the flame (Severino *et al.*, 2022).

The flame dimension can be evaluated through the scale model due to the relative burner simple geometry. The flame dimensions can be scaled by (Severino *et al.*, 2022): $N = cS\mathrm{Pe}_b/\mathrm{Pe}_c^{1/2}$ in which, c is a factor relative to the flame shape, S is the air-fuel stoichiometric relation, and Pe_b and Pe_c represent the Péclet numbers for fuel and impinging oxidizer flows, respectively. Considering an infinitely fast one-step irreversible chemical reaction, $\mathrm{F} + s\,\mathrm{O} \longrightarrow (1 + s)\,\mathrm{P}$, in which F, O and P denote fuel, oxidizer and products, respectively, and s is the stoichiometric coefficient (units of mass). The air-fuel stoichiometric relation is defined as $S = s\hat{Y}_F/\hat{Y}_O$, in which $\hat{Y}_O$, and $\hat{Y}_F$ are the mass fractions of fuel and oxidizer, respectively. The hat on the symbols ($\hat{}$) is used to represent dimensional quantities. The Peclet numbers based on fuel and impinging oxidizer flows are given, respectively, as $Pe_b = \hat{u}_b\hat{R}/\hat{\alpha}$ and $Pe_c = \hat{a}\hat{R}^2/\hat{\alpha}$, in which $\hat{u}_b$ is the fuel velocity, $\hat{R}$ is the burner radius, $\hat{\alpha}$ is the thermal diffusivity, and $\hat{a} = 2\hat{u}_\infty/\hat{L}$ is the strain rate of the counterflow.

A new experimental setup was constructed to obtain the double Tsuji flame. In the present analyses, a single value for Pe_c and three different values for Pe_b are considered. A numerical simulation performed on Fluent®with the GRI3.0 as the kinetic model and Fick's Law as the species transport model.

2. EXPERIMENTAL SETUP

The experimental setup is mainly composed of a sintered bronze cylinder (burner) and two air suppliers, as shown schematically in Fig. 1. The sintered cylinder guarantees a uniform radial velocity profile for fuel. It has an outer diameter of $9.5\,\mathrm{mm}$ and an inner diameter of $4.5\,\mathrm{mm}$ with $30\,\mathrm{mm}$ of length. A radial coflow of nitrogen (N_2) is placed at the end of the cylinder to isolate the fuel stream from oxidizer contamination in the axial direction. Therefore, the oxidizer carried to the flame originates only from the air supplier. A water tube passes concentrically into the burner to maintain the fuel inlet at a constant temperature. Mass flow controllers (MFC) are used to adjust the fuel and nitrogen flow rates. MFC's fuel has a range of 0-5 $\mathrm{L\,min^{-1}}$ and an MFC with a range of 0-50 $\mathrm{L\,min^{-1}}$ was used for nitrogen. The accuracy of the controllers is 2% of full scale.

Two divergent nozzles are placed oppositely to each other to supply the oxidizer counterflow (refer to Fig. 1). The dimensions are an inlet diameter of $23.4\,\mathrm{mm}$ and an outlet area of $400\,\mathrm{cm}^2$. For uniformization of the oxidizer velocity profile, two mesh layers were used. The first layer consists of a $24\,\mathrm{mm}$ height plate full of silica spheres of 2 - $3\,\mathrm{mm}$ diameter placed at $16\,\mathrm{mm}$ from the exit area. The second layer is composed of two steel screens (300 mesh) stacked at the outlet exit area. A blower provides the air for both suppliers. The air flow rate is controlled by a single rotameter with a range of 0 - 50 $\mathrm{L\,s^{-1}}$ and an accuracy of 2% of full scale. They are separated by a distance of $50\,\mathrm{mm}$.

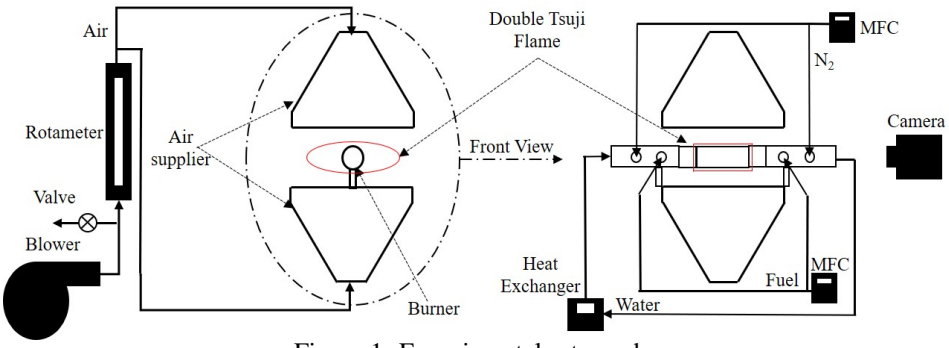

Figure 1: Experimental setup scheme.

3. METHODS

The experimental results encompass three different conditions of Pe_b – namely 1.36, 1.62 and 1.89 –, with methane (CH_4) as fuel. The impinging oxidizer flow is fixed to $18\,\mathrm{L\,s^{-1}}$, which results in a Pe_c of 18.42, for all the cases. The experimental results will be compared with a scaling model and numerical analyses, which are described next.

3.1 Experimental measure approach

A CMOS color camera with a resolution of 1280 x 960 and an exposure time of 300 ms is positioned in the burner's axial direction. The flame is measured digitally by pictures. Its position is calculated by the calibration of pixel to distance, which is estimated based on peak pixel values along the radial direction. The flame location was obtained by the position of the half maximum pixel value. There will be two positions of half maximum pixel value, named as lower branch and upper branch, that represents the flame thickness. The location of the maximum pixel value will be inside these two branches.

One limitation of this measurement technique is that the positioning of the camera (axially to the burner) cannot detect flame variations in the axial direction, as photographs integrate all luminosity in one plane. Moreover, the calibration from pixel to distance and the peak value of pixels are sources of uncertainty that are not taken into account here. However, this measurement method is appropriate to the objectives of this work and provides good physical insights into this novel burner configuration.

3.2 Scaling model

A scaling model is obtained considering a potential flow formulation. The velocity field of the oxidizer is $(\hat{u}, \hat{v}) = (\hat{a}\hat{x}, -\hat{a}\hat{y})$ – i.e., a counterflow –, whose diffusion time ($\hat{t}_d = \hat{R}^2/\hat{\alpha}$) is considered to be equal to the residence time of the fuel on the horizontal symmetry axis ($y = 0$) ($\hat{t}_r = ln(L_x)/\hat{a}$). The flame shape is considered a wedge, and all the ejected fuel burns stoichiometrically with the oxidizer, only transported by diffusion, in the hypotenuse of the triangular flame. The dimensionless length ($L_x \coloneqq \hat{L}_x/R$) and height ($L_y \coloneqq \hat{L_y}/R$) of the flame are given respectively by,

$$Nln(L_x) = L_x \tag{1a}$$

$$L_y = ln(L_x)/\mathrm{Pe}_c^{1/2} \tag{1b}$$

For further details, it is recommended to consult the original article (Severino *et al.*, 2022).

3.3 Numerical analyses

The numerical simulations employ Fluent®v2.21 software (Fluent, 2021). The chemical and species transport models are GRI3.0 and Fick's Law, respectively. If a sufficiently long cylindrical burner is considered, the double Tsuji flame can be treated as a 2D system. Also, the simulations can be limited to just one quadrant of the domain due to the counterflow symmetry. For the inlet of oxidizer and fuel, a boundary condition of uniform velocity is specified orthogonally to the surface at a prescribed temperature of 300 K ($\hat{T}_0$). The mesh size is 200 μm, with refinement taking place in regions with strong gradients (where mesh size is 42 μm), i.e., around horizontal and vertical symmetry axis and near the burner. This approach culminates in an appropriate description of the flame dimensions. Figure 2 shows the numerical domain with the mesh sizes.

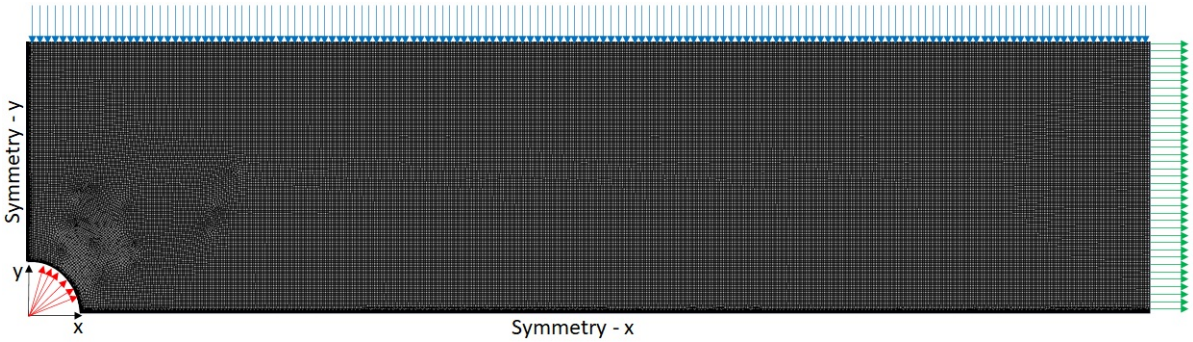

Figure 2: Numerical representation of the physical domain. The red (blue) arrows represent the velocity of the fuel (oxidizer) at the inlet boundary, and the green arrows, at the outlet boundary.

The verification of the model is done with the classical counterflow. Fluent®v2.21 results are compared with the 1D

model results on the vertical symmetry axis. They show a better agreement for higher strain rates due to lower diffusion in the x-direction, which distinguishes the results from the 1D model to the 2D model. The relative error for the highest temperature coordinate is 1.13%.

4. RESULTS AND DISCUSSIONS

Figure 3 shows the front and side views of the double Tsuji flame for Pe_b = 1.89. Note that in Fig. 3a only the right side of the flame is shown; the lower part is blocked by the pipe system that feeds the fuel into the burner. In the middle right of this illustration, an orange area appears, indicating soot formation at the flame tip. In the other two conditions (i.e. Pe_b equals to 1.36 and 1.62), this region is not observed. Figure 3b shows an irregular flame shape upwards of the burner. It is very likely that it is due to irregularities in the oxidation flow, but further investigations are needed. Furthermore, Figure 3 exhibits a thickness of the chemiluminescence, which should represent the flame itself, since the blue color can be associated with the flame reaction zone. However, further analyses must ensure this statement, since, as explained in the methods section, the side view does not capture the flame variations on the z-axis. Thus, for example, in Fig. Figure 3a, it is not possible to observe the flame irregularity at the burner upwards, as shown in Fig. 3b.

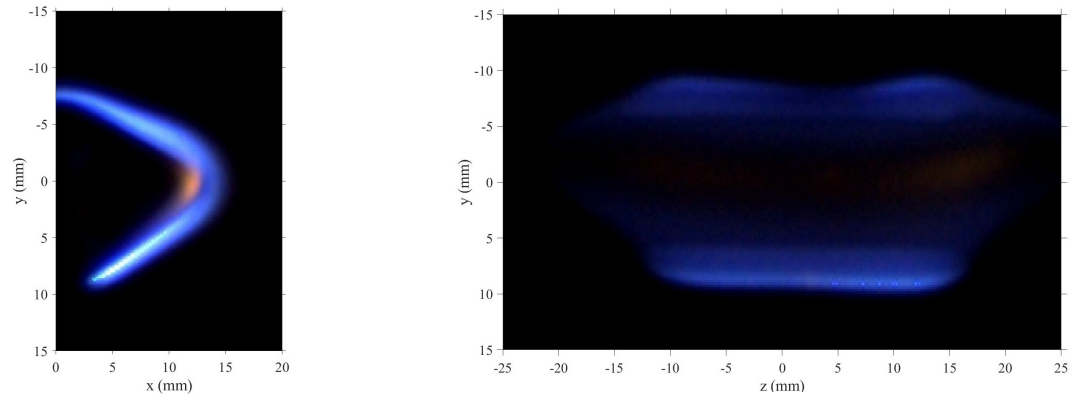

(a) Side view.

(b) Front view.

Figure 3: Photographic images of the flame for $\mathrm{Pe}_b = 1.89$.

The experimental results of flame's length and height together with the estimation calculated by the scale model are presented in Table 1. The flame dimension from the scale model is related to a constant c. According to, Severino *et al.* (2022) for cases where Pe_c is much larger than Pe_b the flame is better shaped by an ellipse ($c = 2$) than a wedge ($c = \pi/2$) which is the case of this work, so $c = 2$ was used.

Pe_b	Experimental - L_x		Experimental - L_y		Scale model	
	Lower branch	Upper branch	Lower branch	Upper branch	L_x	L_y
1.36	2.26	2.72	1.29	1.63	2.11	1.023
1.62	2.39	2.92	1.43	1.73	2.09	1.019
1.89	2.51	3.14	1.54	1.84	2.07	1.016

Table 1: Flame dimension normalized by the burner's radius.

For the experimental results, there is an increase in flame dimensions (length and height) with the increase in the Pe_b. The increase in Pe_b is related to the increase in the fuel velocity in the experiments, consequently, the flame will be more distant from the burner surface, which results in an increase in both branches, lower and upper.

It is noticed that the theoretical model flame length and height does not change significantly in this Pe_b range. The scale model predicts well the lower branch, and the deviation from the experimental result increase with the Pe_b. Indeed, the theoretical model does not change significantly with the increase of the fuel injection, meanwhile, the experimental branches will move away from the burner surface, which will result in a bigger deviation between the both results. For $Pe_b = 1.36$ the deviation is 6.72% and for $Pe_b = 1.89$ the deviation is 17.56 %. For the flame height the deviation is bigger, for $Pe_b = 1.89$ the value of 34.15 % was found. Despite the simplicity of the scale model, the flame length and height can be qualitatively predicted.

Figure 4 shows the numerical results of the normalized fuel fraction ($Y_F = \hat{Y}_f/\hat{Y}_{fb}$), oxidizer fraction ($Y_O = \hat{Y}_o/\hat{Y}_{O\infty}$ and temperature ($T = \hat{T}/\hat{T}_0$) together with the experimental branches and the stagnation point at the symmetry-y. The

x-axis is given by the log function of the normalized distance ($log(y/r_b)$). For brevity, only the case of $Pe_b = 1.63$ is shown, the other cases of $Pe_b = 1.32, 1.89$ follow the same tendency.

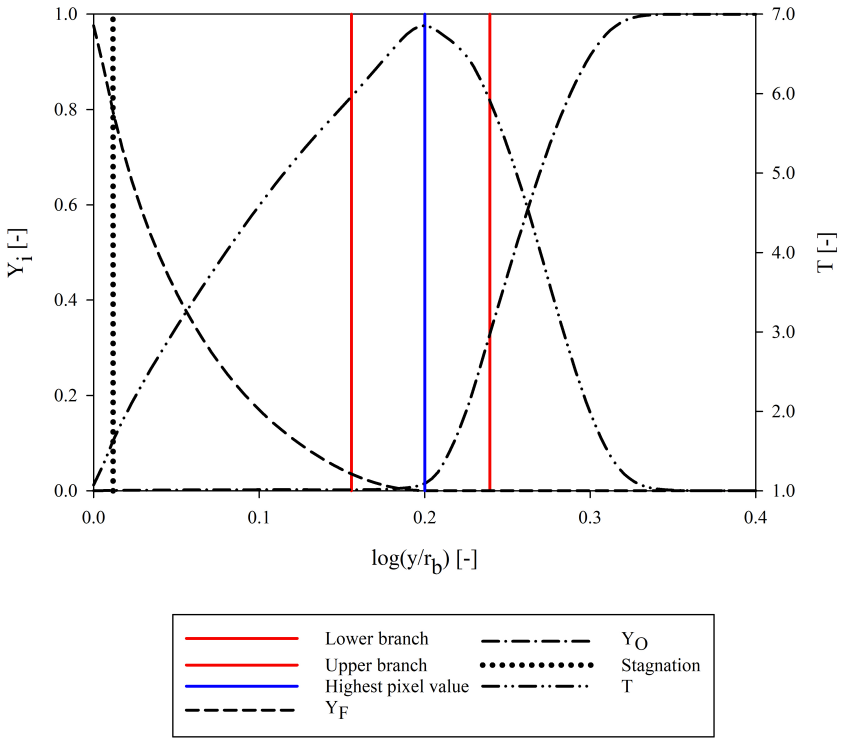

Figure 4: Results on the symmetry-y for $Pe_b = 1.63$.

The stagnation point is at the left of the lower branch (fuel side), as expected, because in counterflow flames with no fuel dilution, the stagnation point is located at the fuel side. Also, the stagnation point is close to the burner surface due to the low fuel velocity in comparison with the oxidizer velocity. The coordinate that fuel and oxidizer mass fraction is consumed, and the temperature peak are between the lower and the upper branch. This shows that the experimental results are agreeing with the numerical results.

Moreover, the coordinate of the highest pix value is near the temperature peak of the numerical result. It is expected that a higher temperature emits more luminosity than a lower temperature, which will result in a higher pixel value. The deviation between the coordinate of the temperature peak and the highest pix value are presented in Table 2, which $T_y = log(y_t/r_b)$, $HP_y = log(y_{hp}/r_b)$ and the deviation (ϵ) between them . Note that, y_t is the location of the temperature peak and y_{hp} is the location of the highest pix value branch.

Pe_b [-]	HP_y [-]	T_y [-]	$\epsilon[\%]$
1.36	0.1728	0.1915	9.78
1.63	0.2001	0.1969	0.72
1.89	0.2250	0.2128	5.71

Table 2: Locations of the temperature peak and the highest pix value location

Figure 5 shows the numerical result for the normalized fuel fraction and the normalized temperature (same definition as Fig. 4) together with the experimental branches on the symmetry-x for $Pe_b = 1.36$. Only the fuel mass fraction is presented in Fig. 5 because the symmetry-x is composed by a coflow configuration, so it is not possible to observe the consumption of the oxidizer mass fraction in the opposed direction of the fuel flow. The abscissa axis is the logarithmic function of the normalized distance in the symmetry-x (x/r_b).

From Figure 5, it is observed that the fuel's entire consumption is outside the experimental branches, far away from the burner. This is a result of the problem's 3D geometry that the 2D numerical simulation does not predict. In the 3D flame, the oxidizer reaches the flame by diffusion in all directions, which does not occur in the 2D domain. In the latter, the oxidizer is provided to the flame only in the xy plane. Therefore, it will take a long time to fuel be consumed in the 2D case, consequently, the flame length will be larger. The numerical result on symmetry-x will overestimate the real flame length.

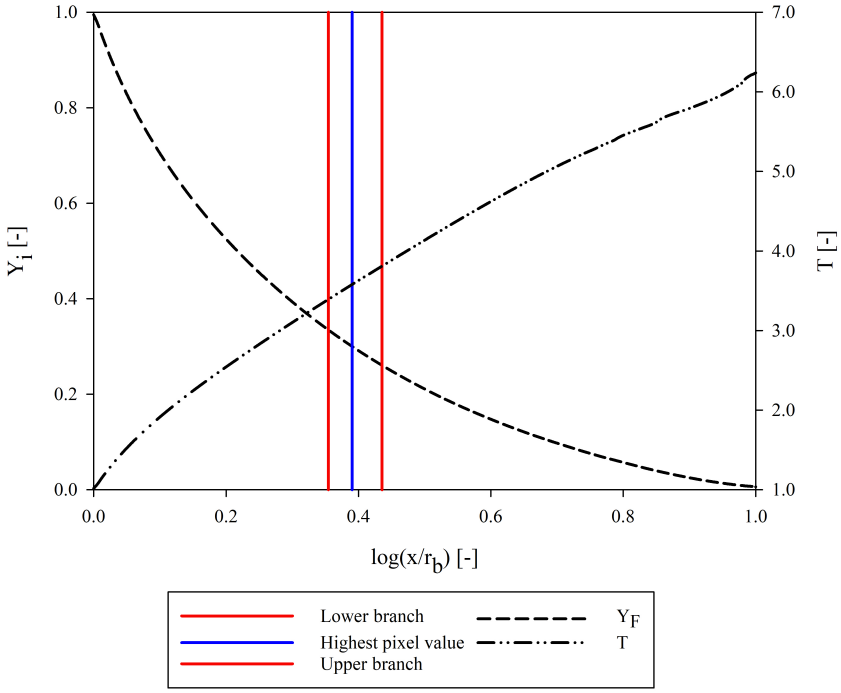

Figure 5: Numerical results on the symmetry-x for $Pe_b = 1.36$

5. CONCLUSION

An experimental setup was constructed to obtain the double Tsuji flames. Their dimensions were obtained in three different fuel flow velocity conditions through a scale model, numerical simulation and an experimental approach. The experimental result shows good agreement with the scale model, despite the model's simplicity. The results' deviation was less than 20 % for flame length and less than 35% for flame height. In the symmetry-y, the numerical result is inside the experimental flame thickness. The highest pixel location and the numerical temperature peak are closer to each other. In the symmetry-x, the numerical result will overestimate the flame length because the model does not predict the z-axis oxidizer component. Finally, the numerical simulation and the scale model can predict well the flame dimension of the double Tsuji burner.

6. ACKNOWLEDGEMENTS

This work was supported in part by Coordenação de Aperfeiçoamento de Pessoal de Nível Superior, Brasil (CAPES), Finance code: 001, by Conselho Nacional de Desenvolvimento Científico e Tecnológico (CNPq) under grants 302717/2016-1, 307922/2019-7 and 161887/2021-0, and by São Paulo Research Foundation (FAPESP) under grant 2021/09246-9.

7. REFERENCES

Bianchin, R., Donini, M., Cristaldo, C. and Fachini, F., 2019. "On the global structure and asymptotic stability of low-stretch diffusion flame: forced convection". *Proc. Combust. Inst.*, Vol. 37, pp. 1903–1910.

Donini, M., Cristaldo, C. and Fachini, F., 2020. "Buoyant Tsuji diffusion flames: global flame structure and flow field". *J. Fluid Mech.*, Vol. 895.

Fluent, 2021. *Fluent 2022 User's Guide*. Ansys.

Severino, M., Donini, M. and Fachini, F., 2021. "Dynamics of diffusion flames in a very low strain rate flow field: from transient one-dimensional to stationary two-dimensional regime". *Combustion Theory and Modelling*, Vol. 25, No. 5, pp. 861 – 888.

Severino, M., Donini, M. and Fachini, F., 2022. "Mathematical modelling of diffusion flames with continuous geometric variation between counterflow and coflow regimes". *Applied Mathematical Modelling*, Vol. 106, pp. 659–681.

Tsuji, H., 1982. "Counterflow diffusion flames". *Prog. Energy and Combust. Sci.*, Vol. 8, pp. 93–119.

Tsuji, H. and Yamaoka, I., 1967. "The counterflow diffusion flame in the forward stagnation region of a porous cylinder". *Symposium (Int.) on Combustion*, Vol. 11, pp. 979–984.

Tsuji, H. and Yamaoka, I., 1969. "The structure of counterflow diffusion flames in the forward stagnation region of a porous cylinder". Vol. 12, pp. 997–1005.

Tsuji, H. and Yamaoka, I., 1971. "Structure analysis of counterflow diffusion flames in the forward stagnation region of a porous cylinder". *Symposium (Int.) on Combustion*, Vol. 13, pp. 723–731.

8. RESPONSIBILITY NOTICE

The authors are solely responsible for the printed material included in this paper.